EFFECT OF XENON BOMBARDMENT ON RUTHENIUM-COATED GRAZING INCIDENCE COLLECTOR MIRROR LIFETIME FOR EUV LITHOGRAPHY

M. Nieto, J. P. Allain, V. Titov, M. R. Hendricks, A. Hassanein, D. Rokusek, C. Chrobak
Argonne National Laboratory, Argonne, Illinois

C. Tarrio, Y. Barad, S. Grantham, T. Lucatorto
National Institute of Standards and Technology, Gaithersburg, Maryland

B. Rice
Intel Corporation, Hillsboro, Oregon

Abstract

The effect of energetic Xenon ion bombardment on the extreme ultraviolet (EUV) reflectivity performance of mirrors is of vital importance for the performance of discharge- and laser-produced plasma extreme ultraviolet lithography (EUVL) sources. To study these effects, we measured absolute and relative reflectivities at the National Institute of Standards and Technology and the Interaction of Materials with Particles and Components Testing facility, to quantify the effects of singly ionized Xe ion bombardment on the reflectivity of Ru EUV mirrors. Results show that unity sputtering is reached at Xe^+ energies near 400-500 eV. The Xe^+-induced sputter yield decreases an order of magnitude with only a 60% decrease in energy. Incident angle-dependent data of Xe^+ bombardment show that the sputter yield is weakly dependent on angle at energies near 1 keV. Dynamic measurements of in situ EUV reflectivity during Xe^+ irradiation show that the oxygen state of the reflecting mirror has a significant effect on reflectivity performance. For example, 13.5 nm light reflecting from an oxygen-rich mirror

results in over a 40% loss in reflectivity. These studies also found that the surface roughness increased only at the atomic scale (subnanometer scale) when exposed to energetic Xe^+ and thus did not contribute to EUV reflectivity losses except for cases of very high fluences ($>10^{16}$ cm^{-2}).

PACS codes: 78.20.Ci, 78.66.Sq, 41.75.Ak, 68.35.Ct, 81.16.Nd.

Keywords: extreme ultraviolet lithography, sputtering, in situ EUV reflectometry

Corresponding author: Martin Nieto, e-mail: nieto@anl.gov

Introduction

The semiconductor manufacturing industry is facing one of its greatest technological challenges. Driven by the need to market faster computers at competitive prices, the semiconductor industry has been consistently shrinking the size of features imprinted in silicon wafers in order to increase the density of components. The industry has reached a point where the size of features to be printed is smaller than the illuminating light wavelength used in optical lithography, the standard process to produce features on Si wafers.[1] One way to continue shrinking feature sizes is the reduction of the light wavelength used in the lithographic process, which is currently 193 nm. The most likely wavelength for the next generation of lithography is 13.5 nm, which lies on the extreme ultraviolet (EUV) band of the electromagnetic spectrum. This introduces numerous technological challenges, for example, the replacement of transmitting lenses with reflecting mirrors within the patterning tool.

EUV light is strongly absorbed by most materials, and producing it at the levels required for high-volume manufacturing is proving quite difficult. In-band EUV power levels on the order

of 1 kW in 2π are required to process 100 wafers per hour at a wafer stage scan speed of 170 mm/s.[2] EUV sources rely on the formation of hot dense plasma either by pinching an electric discharge [3] or by heating targets with very high power lasers.[4] The plasma generated by either method should contain atoms that have strong atomic transitions to produce 13.5 nm photons, such as Xe, Sn, or Li.[5-7] Of all these candidates, Xe has the advantage of being a noncondensable inert gas, which makes it attractive for generating EUV light from discharge-produced plasma (DPP) or laser-produced plasma (LPP). In fact, early-generation commercial EUV lithography tools will likely use Xe EUV radiators as the source.

One of the critical components in an EUVL source is the collector mirror or first condenser optics that faces the EUV-generating plasma. The plasma-facing mirror collects the EUV light coming from the hot dense plasma, focusing it onto the illuminator and projection optics. Depending on the type of source, collector mirrors have different architectures and configurations. For DPP sources, single-layer Ru or Pd mirrors reflect the EUV light incident at grazing angles, typically below 20°. [4,8] For LPP sources, multilayered mirrors (Mo/Si) reflect the light at near-normal incidence. [9] Effects of ion irradiation on the performance of multilayer mirrors (MLM) are covered in separate papers.[10,11] Since the collector mirror is the component closest to the source, it will receive most of the excess (non-EUV) power coming from the hot dense plasma in two forms:

- Out-of-band radiation: any electromagnetic radiation with wavelength falling outside the in-band radiation, defined as 13.5 nm ± 2%.[12] Most of the out-of-band radiation power is deposited in the collector as thermal energy.

- Particle bombardment: energetic particles, both charged and neutral, can leave the hot dense plasma and deposit their energy in the collector.[13,14] This power deposition leads to internal damage and erosion of the collector optics.

Because of its proximity to the source, the collector mirror surface is one of the components that receives the most damage from source operation. This fact leads to critical questions regarding collector optics, such as: What is the lifetime of the collector? Which conditions cause the most damage to the collector? How can collector damage be minimized? To date, the interaction of energetic ions with EUV collector optics has not been studied systematically in order to be able to address these questions adequately. The work we present here seeks to address this situation by carefully examining the effect of ion bombardment on the reflectivity performance of collector mirror optics.

The Interaction of Materials with Particles and Components Testing (IMPACT) facility at Argonne National Laboratory collaborates closely with both EUV source suppliers and semiconductor manufacturers. Studies of the effect of ion bombardment on collector mirrors are performed in IMPACT, measuring mirror erosion and surface modification due to heavy-ion bombardment. In previous work we discussed our findings for multilayered mirrors,[10] typical of LPP sources. In the present work, we discuss the effect of Xe^+ bombardment on single-layer Ru mirrors under different conditions of particle flux, particle energy, and mirror temperature. Measurements of total erosion, surface composition, atomic-scale surface roughness, and x-ray reflectivity were performed on exposed and non-exposed mirror samples.

Experimental Setup

IMPACT is the first experimental facility of the Particle and Radiation Interactions with Matter Experiments facility, recently built at Argonne for measuring and testing high-intensity charged-particle interactions with multicomponent systems. Figure 1 presents an internal view of the experimental chamber, where base pressures between 10^{-9} and 10^{-8} torr (1 torr = 133 Pa) are routinely achieved. The sample is inserted in the chamber via a loadlock system and placed in a sample holder equipped with a resistive heater capable of reaching temperatures up to 500 °C, heating the sample via radiative coupling.

IMPACT is equipped with extensive in situ metrology techniques that include low-energy ion scattering spectroscopy (ISS), Auger electron spectroscopy (AES), X-ray photoelectron spectroscopy (XPS), and extreme ultraviolet photoelectron spectroscopy (EUPS). All of these techniques can probe the sample during exposure to ion beam bombardment or some other treatment. ISS gives information about the composition of the first monolayer in the sample by looking at the energy of incident ions scattered at a particular angle. Because of the high neutralization probabilities of inert gas ion species scattered from metal surfaces, only the ions that interact with the top monolayer are detected. In the case of AES and XPS, the subsurface layers can be analyzed because of the deeper probing depth of electrons and X-rays in the material. The two techniques are complementary, allowing a more reliable identification of components as well as composition and chemical state. The detector consists of a SPECS GmbH PHOIBOS[†] hemispherical electrostatic energy analyzer that records the spectra of both negative particles (electrons) and positive particles (ions) in the kinetic energy range between 0.1 eV and

[†] Commercial products are mentioned for experimental clarity. Mention of commercial products does not imply endorsement by NIST nor by the federal government.

3500 eV. The analyzer is equipped with a five-channel detector with minimum step widths of 7 meV with very small ripple when operated at energies below 400 eV.

The IMPACT chamber is also furnished with an in-situ EUV reflectometer, described in detail elsewhere,[15] which allows the measurement of real-time relative reflectivity as the sample is being modified. The EUV reflectometer uses a Roentgen-type source with a silicon cathode manufactured by Phoenix X-ray GmbH,[†] which emits the spectra shown in Figure 2. The source emits radiation with a peak wavelength 13.5 nm, corresponding to the *2p* transition in Si. More details on the source design and performance are available in the literature.[16] An ellipsoidal mirror coated with 500 nm Ru focuses the light cone coming out of the source aperture onto the sample center, giving a millimeter-size spot on the sample surface. When the sample is tilted at 45° ± 2° (all uncertainties are expressed as standard uncertainties with coverage factor k=1) with respect to the incident ion beam, the light cone centerline is incident at 15° ± 2° with respect to the sample plane, and the specular reflection of this light is captured by a photodiode. When the sample is moved completely out of the EUV light path, a second photodiode measures the light intensity output from the source to verify that it is constant. The relative reflectivity change is calculated by monitoring the 15° photodiode during the sample treatment (ion bombardment, vapor deposition, or both) and normalizing to the value measured before the treatment started. If the initial absolute reflectivity of the sample is known, then the absolute reflectivity evolution during the sample modification can be calculated.

The ability to have in situ diagnosis of samples is important for several reasons. A surface under ion irradiation is actively changing during the exposure dose; for example, radiation-

induced segregation will drive certain target components to the surface, while radiation-enhanced diffusion will drive them away from the surface. The content of adsorbates on a given surface and their role in mechanisms such as sputtering and reflection can be assessed only by actively monitoring the surface as it is being irradiated.

The ion source used for material modification and/or erosion is another important element in the operation of IMPACT. The ion source installed for this purpose is a 1401A electron impact ionization ion gun from Nonsequitur Technologies. The source is capable of producing a wide range of beam types of all inert gases and some reactive gases. Spot sizes are typically between 1 mm and 2 mm in diameter, and currents up to a few microamperes can be achieved for energies between 500 eV and 5000 eV, giving ion fluxes between 10^{14} cm^{-2} s^{-1} and 10^{16} cm^{-2} s^{-1}. The flux level can be dropped by rastering the ion beam over a larger target area; this rastering capability is also important to treat larger sample areas if required by other analysis techniques. The raster area is visually calibrated by using a partially oxidized bulk Li sample, which emits 671 nm light from ion-induced fluorescence during Xe^{+} irradiation. This procedure is also used to perform beam alignment and identify which region of the sample is being treated.

Geometrical effects from sample tilting can be taken into account by reducing the raster size in the direction perpendicular to the sample's axis of rotation. A confirmation of the raster area is usually possible after the treatment if a visible "footprint" is left by the ion beam rastering. Beam intensity and size are controlled by selecting the appropriate source parameters. For more precise measurements of the beam size, a retractable Faraday cup with a five-pinhole

plate is used to measure total beam current as well as the spatial current profile of the beam. A beam profile for a typical Xe^+ ion beam obtained by using this Faraday cup is shown in Figure 3.

Ex situ EUV reflectivity measurements were made at the NIST/DARPA EUV Reflectometry Facility, which is fully described in detail in the literature.[17] The monochromator features a 600 mm^{-1} variable-line-spacing grating operating at a 5° grazing angle of incidence. A plane mirror rotates and translates in order to select the desired wavelength. Wavelength is calibrated by using absorption edges of thin-film filters and the 3d absorption in Kr gas. The reflectivity is measured by direct comparison of incident and reflected powers, with normalization done by using a photodiode monitoring the power incident on a slit shifted 5 mm from the exit slit.

Results and Discussion

Collector Mirror Erosion

For grazing single-layer mirrors (SLM), the maximum thickness of the reflective layer is usually limited by mechanical constraints on the film. However, by having a thick layer, the mirror lifetime is extended because it will take longer to deplete it by sputtering. Thicker thin-film layers, however, have a limit. It is a well-known fact in thin-film processing, typically by magnetron sputtering, that very thick films will not be stable (flaking, pealing) even with thin adhesion layers underneath. Figure 4 shows the EUV reflectivity as a function of both the reflective layer thickness and incident angle, calculated with the IMD code.[18] IMD is a computer program developed by D. Windt for modeling optical properties of single- and multilayer films

based on application of Fresnel equations with modifications that account for interface imperfections. The system modeled was a Ru layer with 1 nm surface roughness on top of a Ti substrate with an interface roughness of 0.5 nm. The figure shows that for thin-film thickness below 10 nm, the reflectivity starts to decrease, with the effect more pronounced as the angle increases with respect to the mirror surface. The reason is that in order to satisfy the condition of total external reflection, operation of the mirror depends on momentum transfer at the critical edge, which is dependent on the mirror material's optical properties. This fact will be relevant in assessing what mechanisms are responsible for mirror reflectivity loss under ion irradiation.

In order to obtain accurate estimates of the mirror erosion rate, the sputtering yield must be measured. The erosion velocity of a target material A undergoing bombardment by B particles is given by

$$\frac{dx_A}{dt} = \frac{Y_{sp,AB}\Gamma_B}{n_A}, \tag{1}$$

where dx_A/dt is the erosion rate of material A in units of cm/s, $Y_{sp,AB}$ is the sputtering yield of A by B (dimensionless), Γ_B is the flux of B particles in units of cm^{-2} s^{-1}, and n_A is the number density of A particles in the target in units of cm^{-3}. If the sputtering yield and the film density are known constants, integration of Eq. (1) yields

$$\Delta x_A = \frac{Y_{sp,AB}}{n_A}\int_0^t \Gamma_B(\tau)d\tau = \frac{Y_{sp,AB}\Phi}{n_A}, \tag{2}$$

where Δx_A is the thickness of material A in units of cm eroded during an exposure time of t seconds, or equivalently exposed to a fluence Φ in units of cm^{-2}, defined as the flux, Γ_B, integrated over the exposure time t in seconds. Equation (2) works under the assumption that the surface is not drastically modified by the implanted particles and that the sputtering is invariant over time. Both these conditions are met for low-fluence bombardment ($<10^{16}$ cm^{-2}) of targets with noble gases, which typically have very weak interactions with the target after being implanted. Equation (2) is not valid when approaching film interfaces, since at that point sputtering of components from both regions may occur. For a constant flux, the fluence Φ is simply equal to the product Γt. If the fluence, the sputtering yield, and the atomic density are known, then the eroded thickness of a sample can be calculated. The fluence is a readily available quantity if the ion current, irradiation area, and exposure time are known, but the sputtering yield is usually not readily available. The sputtering yield depends mainly on four factors: the relative masses of A and B, the mass density of the target, the surface binding energy of the target material, and the energy of the incident particles and their angle of incidence.

In this work, the current between the sample and ground is measured in real time with a picoammeter, and the irradiation area is calibrated by using both the Faraday cup and the fluorescence technique described earlier. The sputtering yield is measured in situ by using a quartz crystal microbalance dual crystal unit (QCM-DCU), with one of the crystals exposed to the sputtered flux from the sample and the other shielded as a reference. By measuring the frequency difference between the two crystals, the collected sputtered mass is measured, and from this measurement the sputtering yield is calculated as explained in detail elsewhere.[19] The

advantage in this setup is that during depth profiling the sputter rate is measured in situ and real time during the profile and in conjunction with serial acquisition of the eroded surface composition and chemical state using ISS and XPS, respectively.

Effect of the Erosion Rate on Reflectivity

The first step in evaluating the effect of physical erosion of Ru mirrors by Xe^+ on EUV reflectivity was to measure the sputtering yield of Ru by Xe^+ for energies between 200 eV and 1000 eV at a 45° incident angle in 100 eV increments, and for an incident angle between 0° and 65° with respect to the sample normal at 1 keV in 5° increments. A SLM sample with a Ru layer 10 nm ± 1 nm thick was exposed to a Xe^+ beam incident at 45°, with the energy varied between 200 eV and 1000 eV. The measured sputtering yield is shown in Figure 5, along with measurements for a bulk Ru sample and values computed with the ITMC (Ion Transport in Materials and Compounds) code developed by our group.[20] A similar study was done for the angular dependence of the sputtering yield of Ru SLM by 1 keV Xe^+, and the measured sputtering values are shown in Figure 6, along with predictions from the TRIM-SP (Transport of Ions in Matter – SPuttering) code. Conducting experiments at heavy-ion grazing incidence and impact energies near 1 keV simulates realistic conditions inside EUV source devices. Grazing incident charged particles in both the DPP and LPP sources have been measured to have energies near 1 keV or above.[13,14]

Once the sputtering yield is measured, the erosion rate can be calculated, and the degree of mirror erosion when exposed to Xe^+ bombardment can be quantified. In order to evaluate the effect of mirror erosion on reflectivity, three SLM samples (Ru-99, Ru-101, and Ru-103) with a

10 nm ± 1 nm Ru film on a 5 nm Ti adhesion layer were exposed to a 1 keV Xe^+ beam. The beam current was set to 3 μA, and the sample was exposed over an area of 1 cm x 1 cm by rastering the beam. The Xe^+ flux incident on the samples for these conditions is 5 x 10^{13} cm^{-2} s^{-1}. The exposure conditions are summarized in Table I. Sample Ru-99 was exposed at normal incidence, while the other two were exposed at 60° with respect to the surface normal. Both Ru-99 and Ru-101 were heated to 200 °C before and during exposure. Heating the mirrors simulates conditions in EUVL source devices because only about 1% of total radiation is in the EUV, and the remaining off-band radiation is converted to heat on the collector mirror. Temperatures have been measured to range from 150 to 300 °C in EUVL source devices.

Taking the measured erosion rate listed in Table I and multiplying by the exposure time, we calculated the eroded sample thickness of 8.7 nm for Ru-99, 12 nm for Ru-101, and 13 nm for Ru-103. The Ru-101 and Ru-103 samples are close to the approximate thickness of the original Ru films (about 10 nm). To illustrate the resultant surface composition on these samples, we show in Figure 7 the ISS scans taken after the Xe^+ exposures. A significant reduction on the Ru peak is observed, consistent with the fact that only small amount of Ru remains on the sample because most of the Ru layer is removed at these fluences. The Ti peak from the layer separating the Ru SLM from the Si substrate is dominant in the spectra, and the oxygen content is significantly increased, approaching the stoichiometry of TiO_4 (80% O, 20% Ti). The source of oxygen in the 5-nm Ti adhesion layer is mainly from the SiO_2 interface during and after growth. Complete transition from Ti^0 to Ti^{4+} is evidenced from the measured stochiometry showing that oxygen has fully segregated and oxidized the Ti layer. Oxygen diffusion and passivation by Ti at the interface with SiO_2 are very common, in particular at ultra thin-film Ti/SiO_2 interfaces of 5 nm thickness or less.[21]

The unexposed Ru SLM shows signs of initial oxidation consistent with ruthenium's high affinity for oxygen. The surface atomic fractions for the three samples calculated from the ISS scans are shown in Table II. Figure 6 shows an oblique incidence leading to relatively higher sputter yield than at normal incidence. This result was confirmed by the measured sputter rates listed in Table I. The differences were small, however, primarily because the sputter yield from heavy-ion sputtering has a rather weak dependence with incident angle. In addition, two other important results were discovered in these experiments. First, the surface temperature of the mirror played a minor role on the erosion level and oxygen content during and after irradiation. Although it would be difficult to extrapolate this result to determine how surface impurities evolve over very long times (i.e., conditions in a EUVL source device), one can safely conclude that temperature has a negligible effect on mirror erosion. The second important result is the evolution of surface roughness, or lack thererof, which is important in determining EUV reflectivity performance. Atomic force microscopy measurements of the virgin sample yielded about 0.27 nm rms surface roughness. For all cases of Xe^+-exposed samples, the surface roughness varied only at the atomic scale; that is, the roughness did not grow beyond 1 nm rms.

After Xe^+ exposure in IMPACT, the EUV reflectivity was measured at the NIST-DARPA facility to understand how heavy-ion irradiation affected the absolute at-wavelength 13.5 nm reflectivity. Figure 8 shows the reflectivity response of two exposed samples (Ru-101 and Ru-103) compared to unexposed samples and calculations made from data found on the Center for X-Ray Optics (CXRO) at Lawrence Berkeley Laboratory website for Ru and Ti layers.[22] The relative uncertainty in these measurements is 5%, as a result of scattered light and the large footprint of the EUV beam on the sample. These samples were selected because Ru-99 did not show large changes in either nanometer-scale surface roughness or surface composition.

A drop of 60-70% in reflectivity is observed for the samples with the Ru almost completely removed. The reflectivity is, however, still larger than expected for a pure Ti layer (i.e., complete removal of the Ru film), indicating that some reflective material is left. From the ISS data, we know that the Ru concentration at the surface is 3% or less. In order to determine whether such content of Ru may alter the reflective properties, IMD simulations were performed for a Ru/Ti mixed layer with 3% Ru on top of a 5 nm Ti layer and a Si substrate. Since it is not known over what depth the concentration of Ru drops to zero, the effect of the mixed layer thickness on the reflective properties needs to be determined.

The thickness of the mixed layer was varied between 0 and 10 nm. The results of the simulation, shown in Figure 9, demonstrate that even a 10 nm thick layer reflects less than the 20% found from the EUV reflectivity measurement. Since it is unlikely to have a mixed layer thicker than 10 nm (the implantation zone is < 1 nm, and the damage zone 66% of this depth), the experimental results suggest that the optical properties of the ion-induced mixed layer are different from those of a system without exposure to irradiation. Indeed, we know that the irradiation removed most, if not all, of the Ru mirror layer for the fluence applied. However, the resultant mirror structure still reflected more than a calculation predicted for a pure Ti layer. This result is particularly important because it suggests that heavy-ion irradiation during exposure to Xe plasmas in EUV sources may lead to equilibrium systems able to reflect better than expected over moderate fluence levels. Future work will determine whether such performance is maintained for orders-of-magnitude larger fluxes.

For the three samples discussed so far, only EUV reflectivity measurements before and after Xe^+ bombardment were performed. In order to monitor the EUV reflectivity *dynamically* as a function of eroded thickness for a SLM sample, the IMPACT in situ EUV reflectometer was

used. A 20 nm Ru SLM (measured by X-ray reflectivity and ellipsometry) deposited on a 5 nm Cr adhesion layer on top of a Si substrate was exposed to a Xe^+ flux of $1.3x10^{13}$ cm^{-2} s^{-1} incident at 30° over an area of 0.36 cm^2 for 85 minutes. Every 5 minutes (except for the first two data points, which were taken at 10-minute intervals), the relative reflectivity was measured, along with the surface composition by using ISS. The sputtered flux was calculated during each interval by using the QCM-DCU diagnostic in IMPACT, allowing very accurate calculations of the eroded thickness. The results of these measurements are given in Figure 10, which shows both the relative reflectivity and the surface atomic fraction as a function of eroded thickness. It was confirmed that the thickness of the Ru layer in the mirror is 20 nm, since it is precisely the thickness at which the Cr underlayer starts to appear, as shown in Fig. 10.

According to the measurements, the reflectivity reaches its minimum when nearly 15 nm of the Ru thin-film mirror is removed, equivalent to 75% of the original thickness. This loss of reflectivity was not expected because calculations with IMD of a 5 nm Ru / 5 nm Cr system reflects over 80% from its original reflectivity, as shown with the dash-dot line. Instead, the relative reflectivity value reaches a steady-state value close to that of a pure Cr 5 nm film. This decrease is faster than the one predicted by calculations with the IMD code (see Figure 4) for the case of a pure Ru thin film with only 5 nm thickness. Since ISS data showed high oxygen content in the Ru film over the course of irradiation, IMD calculations were conducted with RuO_2 optical constants. Figure 10 shows the IMD results for a 5 nm layer of RuO_2 with better agreement to the in situ EUV relative reflectivity data. This result suggests that the oxide state of the thin-film mirror plays an important role on the EUV reflectivity together with the loss of the reflective layer during Xe^+ bombardment. Earlier work has also shown that oxygen may be driven to near-surface regions during heavy-ion bombardment.[11] In addition, the exposure

presented in Figure 10 was close to 10^{17} cm^{-2} fluence. Therefore, surface roughness may have evolved to levels beyond 1.0 nm to 1.5 nm rms and thus contributed to additional relative reflectivity loss compared to the 5 nm RuO_2 layer case (relative reflectivity of ~ 55%).

To understand the role of surface roughness, we need to discuss these results further. Three distinct regions are identified and marked in Figure 10. The first region consists of equal stoichiometric amounts of Ru and O according to the ISS data. The probing depth of ISS is about 1 to 2 monolayers. The 13.5 nm light interacts with most of the top two-thirds depth of this wavelength. Hence, the relative reflectivity in Region 1 begins to decrease primarily because the 13.5 nm photons begin to reflect from layers below ~10 nm (Region 2), where the oxygen content is significantly higher (60% or more O) and thus the relative reflectivity should be much lower. An equilibrium is reached whereby the relative reflectivity is dictated more by the underlying Cr film (Region 3), in agreement with IMD simulations. To further illustrate the dependence of EUV reflectivity on oxide content in the Ru mirror at grazing incidence (<20°), we conducted another experiment on a Ru mirror with lower oxygen content.

Figure 11 shows in situ EUV reflectivity and atomic surface fraction during irradiation with 1 keV Xe^+ at normal incidence. The results are convincing. The structure that has nearly a 1:1 ratio of Ru to O (Region 1) reflects as expected and maintains this level of reflectivity because the layers below are less oxygen-rich. The relative reflectivity begins to decrease once the 13.5 nm light begins to interact with the oxygen-rich Ru-Cr interface (Region 2).

Effect of Surface Roughness on Reflectivity

Surface roughness can reduce the reflectivity response of mirror materials, as evidenced by CXRO calculations shown in Figure 12, if the surface reconstruction after irradiation leads to roughness spatial variations larger than about 10% of the photon wavelength. Surface roughness increases diffuse scattering, hence reducing light collection capabilities of curved mirrors. In order to determine the effect on surface roughness induced by ion beam bombardment, a set of Ru thin-film samples was exposed to a Xe^+ beam at 1 keV. In order to avoid reflectivity changes associated with mirror erosion, thicker Ru layer SLMs (80 nm, measured by X-ray reflectivity) were used so that no significant loss of reflective material occurred during the exposure. Results both on thin Ru mirror films (<20 nm; see Table I) and on thicker mirrors indicate that the EUV reflectivity changed very little as long as these surface reconstructions varied at the atomic scale. That is, the surface roughness change was not greater than 1 nm rms.

Four samples were exposed to Xe^+ bombardment at normal incidence; the conditions for the irradiation are tabulated in Table III. A low-current (<100 nA) Xe^+ beam was used to carry out the exposures, which were done for two energies (550 eV and 1300 eV) and two temperatures (25 °C and 80 °C). The rms roughness for the exposed samples over a 1 μm x 1 μm area was measured with an atomic force microscope (AFM), and no significant changes with respect to the unexposed sample were found for any of the conditions described above. In-band EUV reflectivity measurements were performed at Fraunhofer Institut in Aachen by using a grazing incidence reflectometer operating around a 13.5 nm spectral range with a compact xenon pinch plasma light source.[23] The absolute reflectivities measured for all samples averaged 0.78-0.79 at 15° incidence compared to an unexposed sample at 0.78. [24] Since the samples are thick

and the fluence is relatively small, the reflective layer thickness does not change significantly. In-band EUV reflectivity results indicate that the roughness also remains unaltered, as verified by AFM measurements. Moreover, the results also indicate that for the particular conditions of Xe^+ bombardment, the SLM reflectivity performance remains unchanged. Further studies are necessary to determine whether a higher fluence together with an oblique angle of incidence can induce more significant changes to the surface roughness and hence decrease the reflectivity, as suggested by the results from the erosion of the thinner mirror shown in Figure 10.

Conclusions

The reflectivity response of Ru SLM exposed to Xe^+ bombardment was investigated at the IMPACT facility for various conditions simulating the environment in an EUVL source device. Two factors are altered as a result of the exposure of the SLM to fast (1 keV) Xe singly charged ions: the thickness of the reflective layer and the oxide state of the reflective layer. If the fluence is high enough and if surface reconstructions result in changes beyond the atomic scale (>1.5 nm rms surface roughness), then the surface roughness of the collector mirror plays a significant role in decreasing the specular reflectivity response at 13.5 nm, as indicated by CXRO calculations.

Sputtering yield measurements for Xe^+ incident on Ru thin films were performed as a function of energy and angle. For Xe^+ at 500 eV the sputter yield was unity; that is, for every ion incident, a surface atom is sputtered. These rates increase slightly for the glancing incidence of fast ions. The yield drops to 10% with only a 60% drop in energy. This result is significant in terms of operation lifetime of the mirror for Xe-based EUVL sources. A sharp decrease of the absolute reflectivity was found for samples with a reflective layer almost completely eroded by

Xe^+ bombardment. However, this level of reflectivity was better than predicted by computer simulations, likely because of a change in the optical properties of the Ru mirror induced by heavy-ion bombardment. Measurements were also taken of EUV reflectivity as a function of the reflective layer thickness with a novel in situ EUV reflectometer. Measurements indicate that as the 13.5 nm light begins to interact with oxygen-rich regions, its reflected intensity decreases. Comparison of IMD simulations results to real-time in situ EUV reflectivity data indicates that the oxide state of the film determines the loss of reflectivity of the mirror for fluences less than 10^{16} cm^{-2}.

For higher fluence levels, the surface reconstruction leads to enhanced surface roughness beyond the atomic scale, eventually leading to additional reflectivity loss of the Ru SLM. The effect found for the Ti underlayer where the reflectivity was enhanced after irradiation was not observed for the Cr underlayer architecture. Chromium was chosen because of its good adhesive properties to Si and Ru. For low-fluence exposure of thick (>20 nm) Ru mirrors to Xe^+ at normal incidence with two different energies at two different temperatures, no significant changes to the surface roughness were found in AFM and absolute EUV reflectivity measurements. More studies will be carried out to evaluate whether other factors such as angle of incidence or fluence levels have a stronger effect on the mirror surface roughness and consequently the at-wavelength 13.5 nm specular reflectivity.

These studies indicate that Xe as EUV radiator for microlithography is very efficient in removing Ru thin-film mirror layers when exposed to fast Xe^+ particles generated during the plasma discharge. Fluences near and slightly above 10^{16} cm^{-2} will lead to removal of 10 nm Ru SLM and, consequently, loss of reflectivity. Thus, Xe fast-ion and neutral fluxes must remain below 10^8 $cm^{-2}s^{-1}$ for the survival of a 10 nm Ru SLM over the course of about one year of

operation. Where a Ti underlayer is used, the reflectivity drop is not as large as compared to a Cr underlayer. This result indicates that under certain conditions, Xe^+ irradiation can induce changes in the optical properties of the remaining thin-film Ru grazing incidence mirror.

Acknowledgments

We thank P. Zink, C. Metzmacher, and K. Bergmann for at-wavelength reflectivity measurements of thick Ru mirrors listed in Table III. We also thank the Optics Fabrication and Metrology group (incl. Al Macrander, C. Liu, and R. Conley) of the Advanced Photon Source at Argonne for fabrication and characterization of two samples used in this paper. This work was supported in part by the U.S. Department of Energy, under Contract W-31-109-Eng-38, and the NIST Office of Microelectronics Projects.

References

1 J. J. Watkins and D. J. Bishop, MRS Bull. **30,** 937 - 941 (2005).
2 V. Y. Banine and R. Moors, J. Phys. D. **37,** 3207–3212 (2004).
3 W. Neff, K. Bergmanna, O. Rosierb, R. Lebert, and L. Juschkinc, Cont. Plasma Phys. **41,** 589-597 (2001).
4 U. Stamm, J. Phys. D. **37,** 3244–3253 (2004).
5 J. Avitzour, I. Geltner, A. Morozov, Y. Ping, and S. Suckewer, *8th International Conference on X-Ray Lasers*, Aspen, CO, 2002 (AIP), p. 212 -219.
6 A. Sasaki, K. Nishihara, F. Koike, T. Kagawa, T. Nishikawa, K. Fujima, T. Kawamura, and H. Furukawa, IEEE J. Sel. Top. Quantum Electron. **10,** 1307-1314 (2004).
7 A. Hassanein, V. Sizyuk, V. Tolkach, and V. Morozov, J. Microlith. Microfab. Microsyst. **3,** 130-138 (2004).
8 W. N. Partlo, I. V. Fomenkov, R. M. Ness, R. I. Oliver, S. T. Melnychuk, and J. E. Rauch, *Microlithography 2001: Emerging Lithographic Technologies V*, Santa Clara, CA, 2001 (SPIE), p. 232 - 248.
9 S. Bajt, H. N. Chapman, N. Nguyen, J. Alameda, J. C. Robinson, M. Malinowski, E. Gullikson, A. Aguilar, C. Tarrio, and S. Grantham, App. Opt. **42,** 5750 - 5758 (2003).
10 J. P. Allain, A. Hassanein, M. M. C. Allain, B. J. Heuser, M. Nieto, C. Chrobak, D. Rokusek, and B. Rice, Nuclear Instum. Methods Phys. Res. B **242,** 520-522 (2006).
11 J. P. Allain, M. Nieto, and A. Hassanein, in *Preprint* (2006).

[12] F. Bijkerk, L. A. Shmaenok, A. P. Shevelko, R. K. F. J. Bastiaensen, C. Bruineman, and A. G. J. R. van Honk, Microelec. Eng. **27,** 299 - 301 (1995).
[13] A. Endo, IEEE J. Sel. Top. Quantum Electron. **10,** 1298-1306 (2004).
[14] E. L. Antonsen, K. C. Thompson, M. R. Hendricks, D. A. Alman, B. E. Jurczyk, D. N. Ruzic, T. D. Chinh, G. Edwards, S. Wurm, O. Wood, and R. Bristol, *Microlithography 2005 - Emerging Lithography Techniques IX*, San Jose, CA, 2005.
[15] M. Nieto, J. P. Allain, A. Hassanein, M. R. Hendricks, and P. Plotkin, in *Preprint* (2006).
[16] A. Egbert, B. Mader, B. Tkachenko, A. Ostendorf, C. Fallnich, B. N. Chichkov, T. Mißalla, M. C. Schurmann, K. Gabel, G. Schriever, and U. Stamm, J. Microlith. Microfab. Microsyst. **2,** 136-139 (2003).
[17] C. Tarrio, S. Grantham, M. B. Squires, R. E. Vest, and T. B. Lucatorto, J. Res. NIST **108,** 267 - 273 (2003).
[18] D. L. Windt, Comput. Phys. **12,** 360-370 (1998).
[19] J. P. Allain and D. N. Ruzic, Nucl. Fusion **42,** 202 - 210 (2002).
[20] A. Hassanein and D. L. Smith, Nuclear Instum. Methods Phys. Res. B **13,** 225 - 229 (1985).
[21] O. Auciello, W. Fan, B. Kabius, S. Sasha, J. A. Carlisle, R. P. H. Chang, C. López, E. A. Irene, and R. A. Baragiola, App. Phys. Lett. **86,** 042904-1 - 042904-3 (2005).
[22] E. Gullikson (2004) *X-Ray Interactions With Matter.* http://www-cxro.lbl.gov/optical_constants/
[23] K. Bergmann, O. Rosier, and C. Metzmacher, Rev. Sci. Instrum. **76,** 43104 (2005).
[24] P. Zink (2005). Private communication

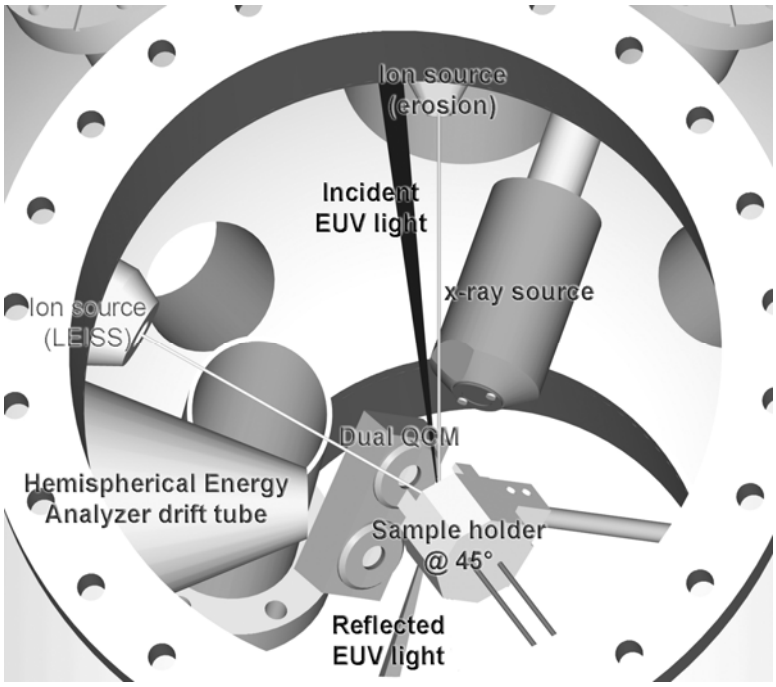

Figure 1. Schematic of the IMPACT (Interaction of Materials with Charged Particles And Components Testing) facility, highlighting the components relevant to the present work.

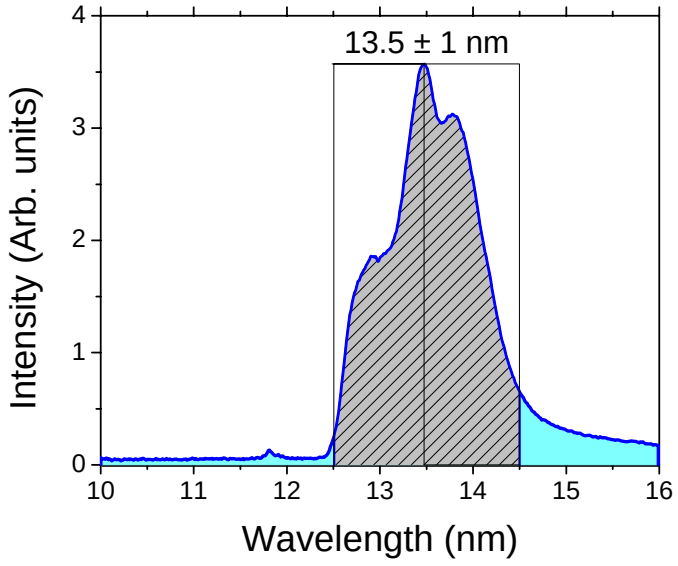

Figure 2. Light spectra emitted from the Phoenix EUV source.

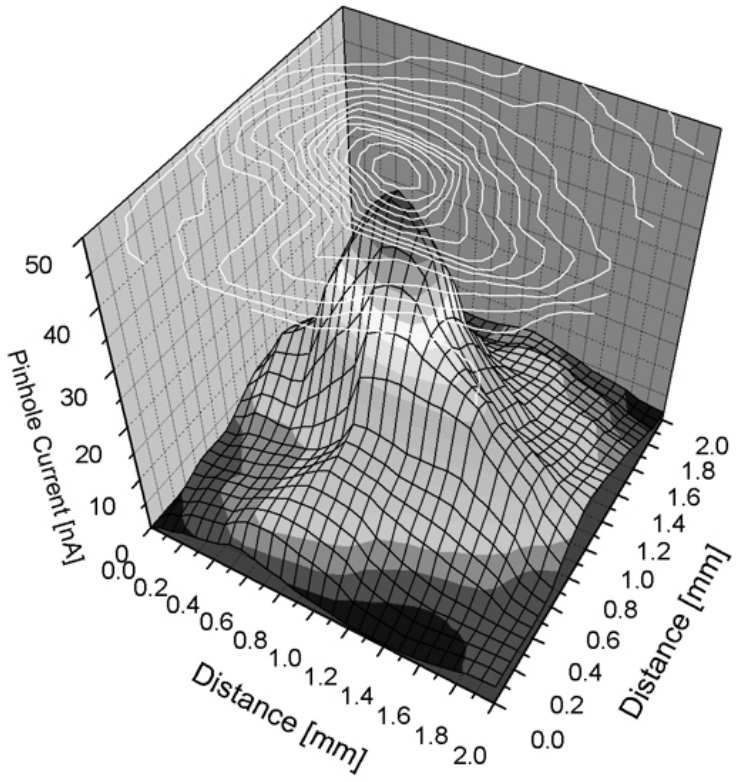

Figure 3. Xe^{+} beam profile for an energy of 1 keV. The diameter of the beam is taken as the FWHM of the Gaussian shape, which is 0.7 mm in this case.

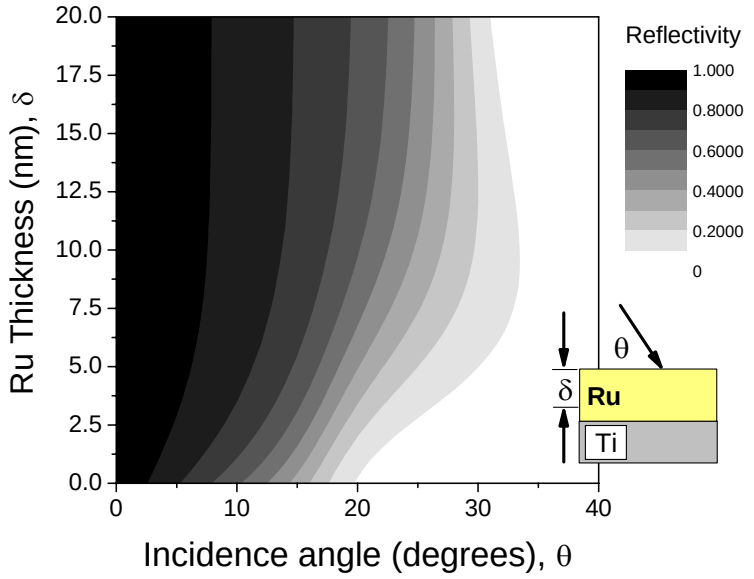

Figure 4. EUV (λ=13.5 nm) reflectivity of a Ru SLM with 1 nm RMS roughness as a function of angle and layer thickness. The Ru layer is on top of a Ti substrate, and the interface has a roughness of 0.5 nm.

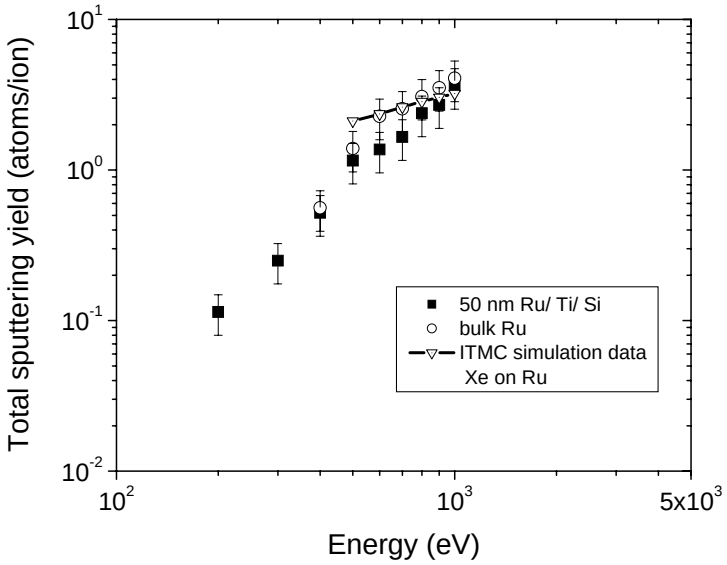

Figure 5. Sputtering yield as a function of Xe^+ energy incident at 45° on a Ru mirror. Comparisons to results from bulk Ru and computations are shown as well.

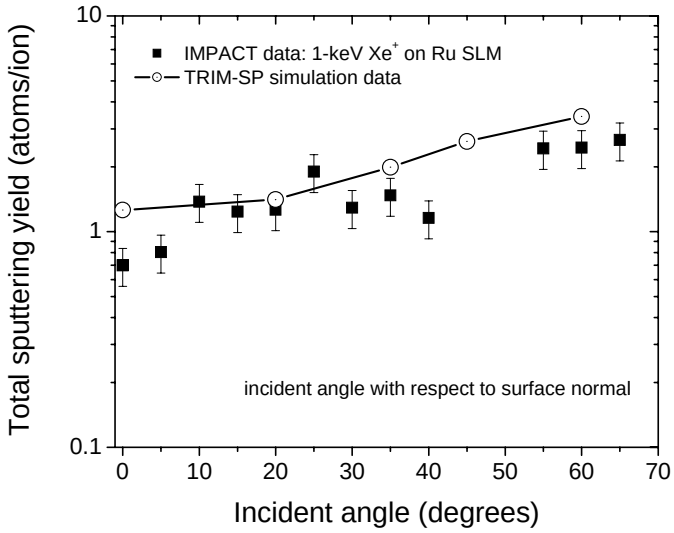

Figure 6. Sputtering yield as a function of 1 keV Xe^+ incident angle (with respect to surface normal) for a Ru mirror. The IMPACT data is compared to TRIM-SP simulation results.

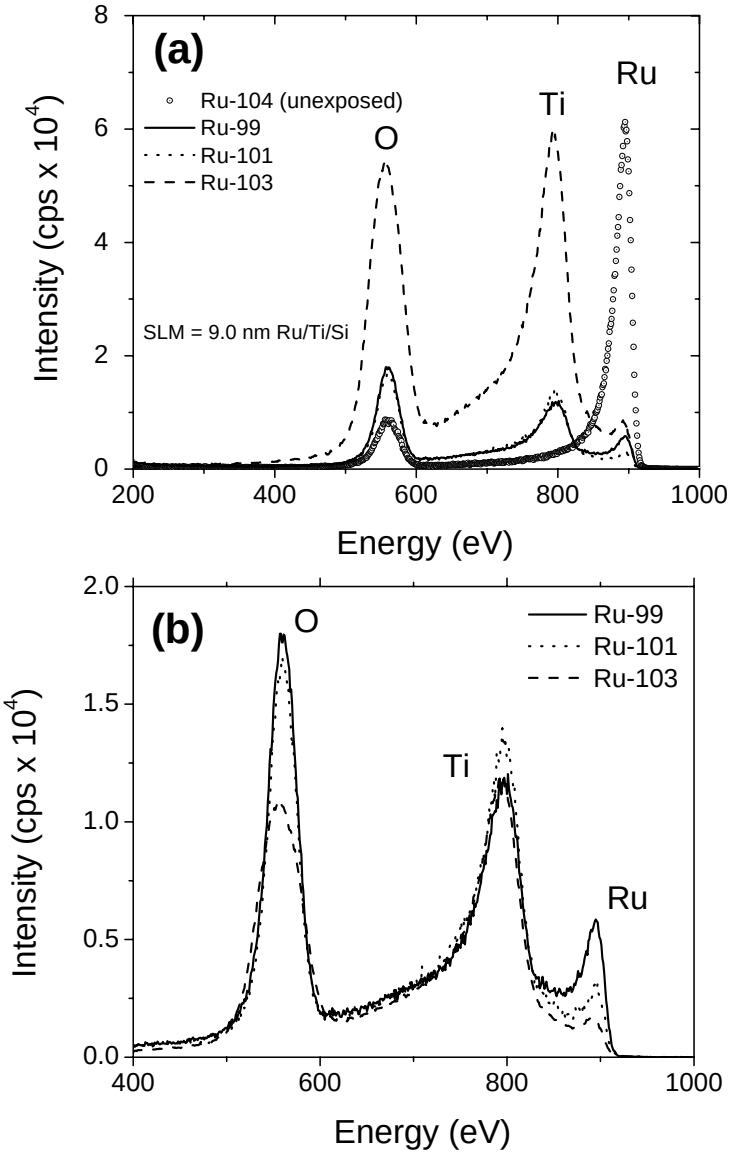

Figure 7. ISS scans for the Ru SLM samples in Table I exposed to Xe^+ bombardment at 1 keV and normal incidence: (a) absolute intensities comparing to the unexposed sample, Ru104, and (b) ISS data normalized to the Ti peak shared by all the irradiated samples.

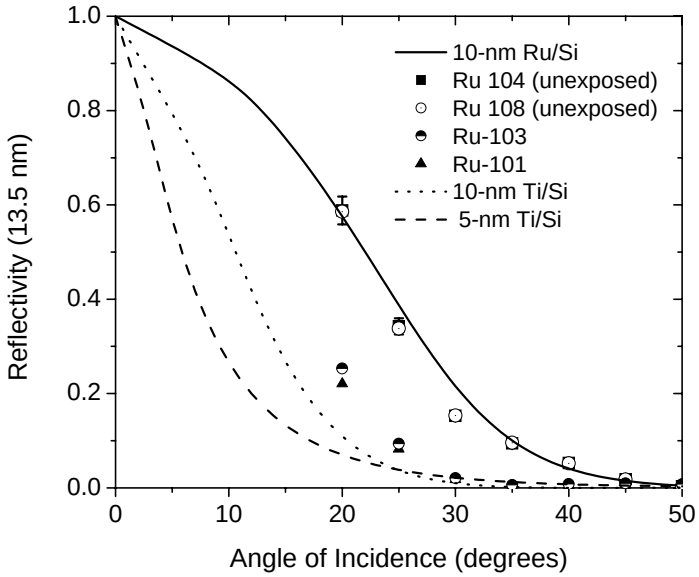

Figure 8. At-wavelength (λ = 13.5 nm) EUV reflectivity for virgin and treated samples as a function of incidence angle. The calculated reflectivity using CXRO for pure 10 nm Ru and Ti layers is shown in the figure with solid and dotted lines, respectively. Dashed lines show results for a 5 nm Ti layer.

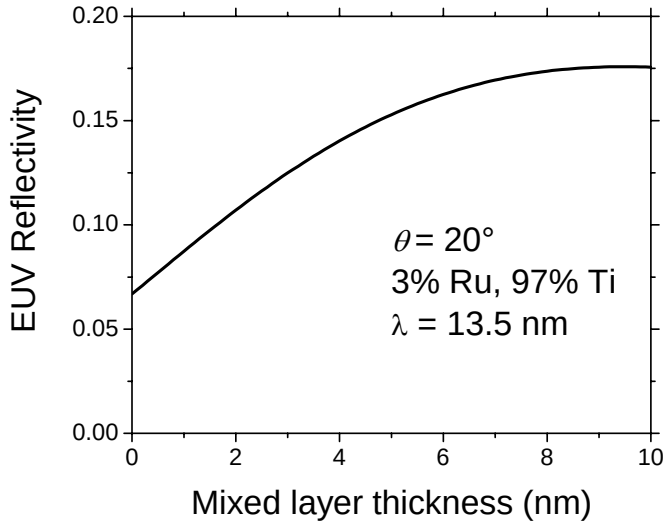

Figure 9. Calculated absolute reflectivity of a mixed 3% Ru 97% Ti layer as a function of the mixed layer thickness. Even at a large thickness (10 nm), the reflectivity does not reach the experimental value > 20% for 20° incidence (see Figure 8).

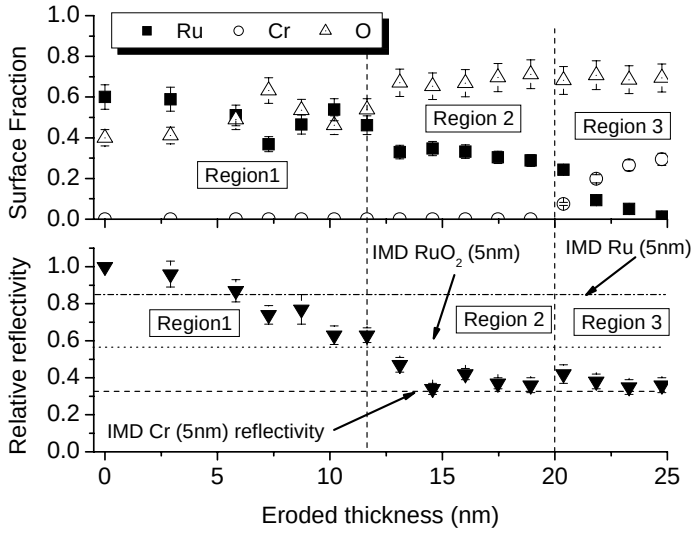

Figure 10. Surface composition and EUV reflectivity as a function of eroded mirror thickness. The dashed horizontal line in the lower panel shows the relative reflectivity of Cr with respect to Ru for 13.5 nm photons at 15° grazing incidence. The dashed vertical line separates three distinct damage and optical regions.

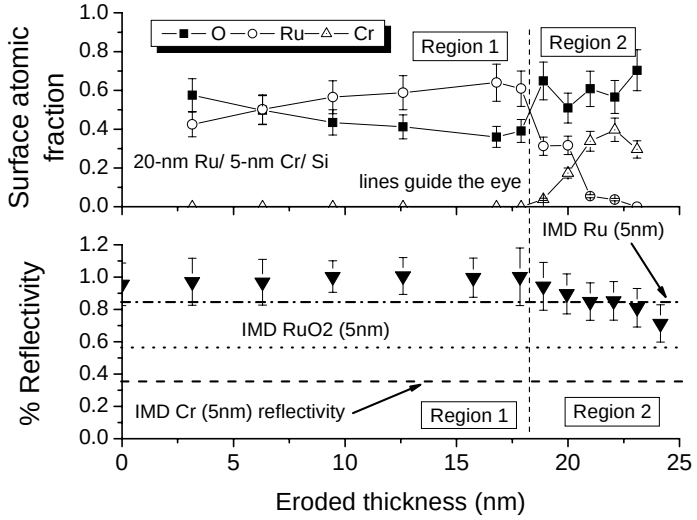

Figure 11. Surface composition and EUV reflectivity as a function of eroded mirror thickness for Ru SLM with relatively lower oxygen content. The dashed horizontal lines in the lower panel show the relative reflectivity of Cr with respect to Ru and RuO_2 for 13.5 nm photons at 15° grazing incidence. The dashed vertical line signals the position of the interface.

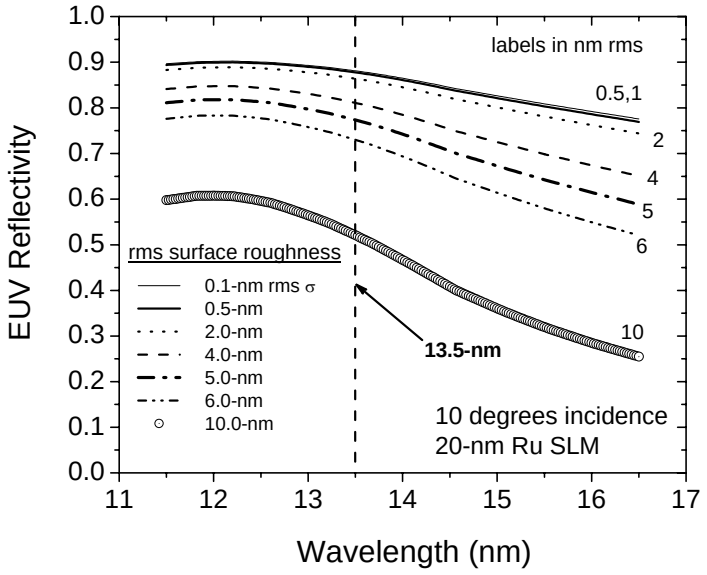

Figure 12. IMD calculations showing the effect of surface roughness on Ru reflectivity.

Table I. Irradiation conditions for the samples evaluated in this study.

Parameter	**Ru-99**	**Ru-101**	**Ru-103**
Xe ion energy (eV)	1000	1000	1000
Angle of Inc. (deg)	0	60	60
Fluence (10^{16} cm^{-2})	5.3	4.8	3.7
Temperature (°C)	200	200	25
Erosion rate (nm/s)	0.0071	0.0105	0.0103
Erosion rate (nm/s) TRIM-SP	0.0080	0.0180	0.0150
Thickness lost (nm)	8.7	12	13
Surface roughness Post-exposure[a] rms (nm) AFM	0.38	0.37	0.36

[a] Pre-exposure atomic force microscopy (AFM) on virgin sample from same batch was 0.27 nm rms for a 1 μm x 1 μm scan in tapping mode. Post-exposure AFM measurements under same conditions.

Table II. Sample surface composition after Xe^+ exposures measured by low-energy ion scattering spectroscopy.

Element	**Ru-99**	**Ru-101**	**Ru-103**	**Virgin**
Oxygen	0.84	0.82	0.80	0.55
Titanium	0.13	0.17	0.19	0
Ruthenium	0.03	0.01	0.01	0.45

Table III. Summary of thick-film SLM exposures to Xe^+ ions with measurements of atomic force microscopy and at-wavelength EUV reflectivity.

Sample ID	**Xe beam energy (eV)**	**Temp. (°C)**	**Fluence (× 10^{15} cm^{-2})**	**Surface Roughness (nm rms)**	**13.5-nm reflectivity 15-deg inc.**
PHL3-7	550	25	8.2	0.78	0.74
PHL3-9	550	80	4.2	0.84	0.78
PHL3-6	1300	25	8.0	2.44	0.73
PHL3-10	1300	80	4.9	1.05	0.74
PHL3-11	unexposed	--	--	1.46	0.75

This work was supported in part by the U.S. Department of Energy under Contract W-31-109-ENG-38.